Original Paper

Melanie Nentwich*

Structure relations in the family of $Hf_xZr_{1-x}O_2$ solid solution

https://doi.org/..., Received ...; accepted ...

Abstract: Hafnium Zirconium Oxide $Hf_xZr_{1-x}O_2$ is a potentially ferroelectric material with high perspectives in semiconductor applications, due to their compatibility with silicon technologies and their low toxicity. Despite their chemical simplicity, the $Hf_xZr_{1-x}O_2$ family comprises a large variety of different phases. We compiled a complete list of experimentally and theoretically reported $Hf_xZr_{1-x}O_2$ structure types. All of them are symmetrically related to the common aristotype with Fluorite structure. The transition paths between those strucutre types have been determined and are presented in a Bärnighausen diagram. Interestingly, not all transitions follow the conventional group-subgroup relations and involve severe atomic shifts indicating martensitic type transitions. Further, the structures were compared to each other in detail regarding the dimensionality of atomic shifts and the accompanied lattice distortions. Finally, the information provided by the Bärnighausen diagram was used to convert the indices of a reflection before and after a phase transition. This conversion allows the study of (dis)appearing reflections during phase transitions.

Keywords: Bärnighausen diagram; phase transition; ferroelectricity; polymorphism

PACS: 61.50.Ah; 61.66.-f; 77.55.+f; 77.55.-g;

1 Curriculum Vitae

***Corresponding author: Melanie Nentwich,** Deutsches Elektronen-Synchrotron DESY, Notkestraße 85, 22607 Hamburg, Germany

Melanie Nentwich studied Mathematics at Universität Leipzig in 2005, switching to Applied Mathematics at the TU Bergakademie Freiberg one year later. She got strongly attracted to her minor subject that focused on resonant X-ray studies of rare earth crystals, which became the topic of her Diplom in 2012. She followed up this research by a PhD in physics in 2020, joining different projects on resonant synchrotron radiation but also on energy storage and conversion. She also supported the working group of Young Crystallographers of the German Crystallogrpahic Association as a Chair and later as main blog author. In the meantime, she gained a lots of experience in managing synchrotron beamtimes, attending and organizing conferences as well as writing proposals for projects and beamtimes. Today, Melanie is a PostDoc at DESY Photon Science, Hamburg, and calculates ray tracing models of future beamlines for the CREMLINplus project.

2 Introduction

The predominant part of the earth's crust consists of diverse oxides that exist in wide varieties implying a great manifold of material properties. For instance, oxides are used as pigments, catalysts, preservatives for food and wine, optical elements, and pyrotechnics. Additionally, they are potentially fire resistant, antibacterial and antifungal, as well as pyro-, piezo-, or ferroelectric. The last mentioned ferroelectrics are a hot topic of current research, especially because the switchable polarity is always accompanied with pyro- (temperature change induces change in polarity) and piezoelectricity (deformation induces change in polarity). All these combined properties open up a wide range of applications, *e. g.* high/permittivity capacitors, ferroelectric memories, pyroelectric sensors, piezoelectric and electrostrictive transductors, electrooptic devices, and PTC thermosistors [1].

The Hafnium Zirconium Oxide family $Hf_xZr_{1-x}O_2$ is a prominent example of oxides. This family includes a frequently discussed structure type with a polar space group allowing ferroelectricity: the orthorhombic group $Pbc2_1$ (29). Single phase, ferroelectric $Hf_xZr_{1-x}O_2$ thin films are a highly desirable materials for semiconductors and nanoelectronics as they are compatible with the silicon technology, its chemistry is simple, it has low toxicity and, whatsmore, most of its ferroelectric phases are more stable for thin films than for bulk [2]. Additionally, annealing-free films are compatible to the CMOS technology (complementary metal-oxide-semiconductor), they can be grown as atomically thin devices at wafer scale, and they have a very low surface roughness [3]. All these properties allow unnumerable applications, *e. g.* as switchable diodes in memory cells [4], or as ferroelectric thin film transistors [3], as microwave devices (for radars and modern

communication like 5G and the internet-of-things), in FETs (field effect transistor; as base for graphene [5] or for negative capacitance FETs [6]), for energy harvesting (electromagnetic energy in microwaves) [5].

Historically, the different phases are often abbreviated by their lattice type symbol, *e. g. m* for monoclinic. However, over the time, more and more phases with the same lattice type were discovered and, thus, had to be extended and are not unique anymore. For instance, the structure type with ferroelectric space group $Pbc2_1$ (29) is addressed as *o*-phase [2, 7], *o*III-phase [8], or FE-*o*-phase [9, 10]. Whatsmore, a crystallographic systematization is missing.

In the present work, we created a comprehensive overview of the different phases of the $Hf_xZr_{1-x}O_2$ family, which has a greater diversity than widely assumed. In total, ten experimentally confirmed structure types exist and additionally 13 more were predicted by DFT [10, 11]. Among all those types are nine with a polar space group allowing ferroelectricity. Here, all structure types were systematically analyzed for their symmetry relations and were arranged in a Bärnighausen diagram. Interestingly, the transitions to the majority of the phases requested an additional kind of transition beside the group-subgroup relations, because severe atomic shifts were involved. These distortions indicate that maternsitic phase transitions are involved.

After gaining an hierarchical overview of the $Hf_xZr_{1-x}O_2$ phases, we carried out a structural comparison between them, revealing super structure relationships between some of the orthorhombic and monoclinic types. Finally, we present a way to convert the reflection indices between two different but related phases, *e. g.* before and after a phase transition. This conversion is based on the information listed in the Bärnighausen diagram and allows the study of (dis)appearing reflections during phase transitions; not only for the $Hf_xZr_{1-x}O_2$ family.

3 Results and Discussion

The heart of the present article is a comprehensive overview of the different structure types within the $Hf_xZr_{1-x}O_2$ family. A literature search revealed ten different, experimentally determined structure types, complemented by 13 further structure types predicted with DFT. These phases show the same structural motives of octahedrally coordinated *M* atoms. The corresponding structural relations "can often be expressed by group-subgroup relations" (GSR) [12], which, however, only describe symmetry relations meaning the transition between space groups (SG) in the first place. The correct linkage between the atomic coordinates always has to be examined carefully before deducing structural relationships [12]. The existance

of a GSR is a necessary precondition for second order phase transition [13], which means that the transition cannot be of second order if no proper GSR exists and that a martensitic transition could be present.

For the present family of structures, a major part of the transition paths can be expressed with capable GSR while considering the correct transition of Wyckoff positions. Those relations include *translationengleiche* (with perpetuation of translational symmetry), *klassengleiche* (with perpetuation of lattice symmetry) and *isomorphous* (with perpetuation of both) transitions. However, some atomic positions cannot be transferred with the group rules in force. For instance, the split of the O position while transitioning from the ordered version of Zirconia ($P4_2/nmc$, 137) to its unordered version (see Sec. 3.1.2) cannot be described with the above three concepts of GSR. Therefore, an additional category of transition is needed. We now categorize the convenient transitions *translationengleich*, *klassengleich*, and *isomorphous* as *coherent* (connected in the sense of GSR) and all other transitions (involving more than "minor" changes) as *incoherent*, following the nomenclature of [14]. Remarkably, a second order phase transition "can only occur, if there is a group-subgroup relation between the space groups of the two crystal structures" [13].

The symmetry relations between the different structure types is visualized with Bärnighausen diagrams. The experimentally confirmed phases of the $Hf_xZr_{1-x}O_2$ compounds (M = Hf, Zr) are displayed in Fig. 1, additional branches also including the phases predicted with DFT are shown in Fig. 2.

Fig. 1 and 2 are very hard to read due to the small font. Maybe you can increase it at the expense of a space between the lines?

The diagrams were extended to present further information beside the standard crystallgraphic data, which include SGs, Wyckoff positions and the kinds of transitions. The extensions involve the information whether the type was confirmed with DFT or experiment, or if the type is auxiliary to complete the diagram. Further indications are added for the structure type, the lattice type, and the dimension of the metal ion displacement with respect to the aristotype (structure type with the highest symmetry).

The following sections will describe the geometrical changes associated with the different symmetry transitions. The Supplementary Material adds a special focus on the *incoherent* transitions. Subsequently, this new knowledge is applied to two brief examples.

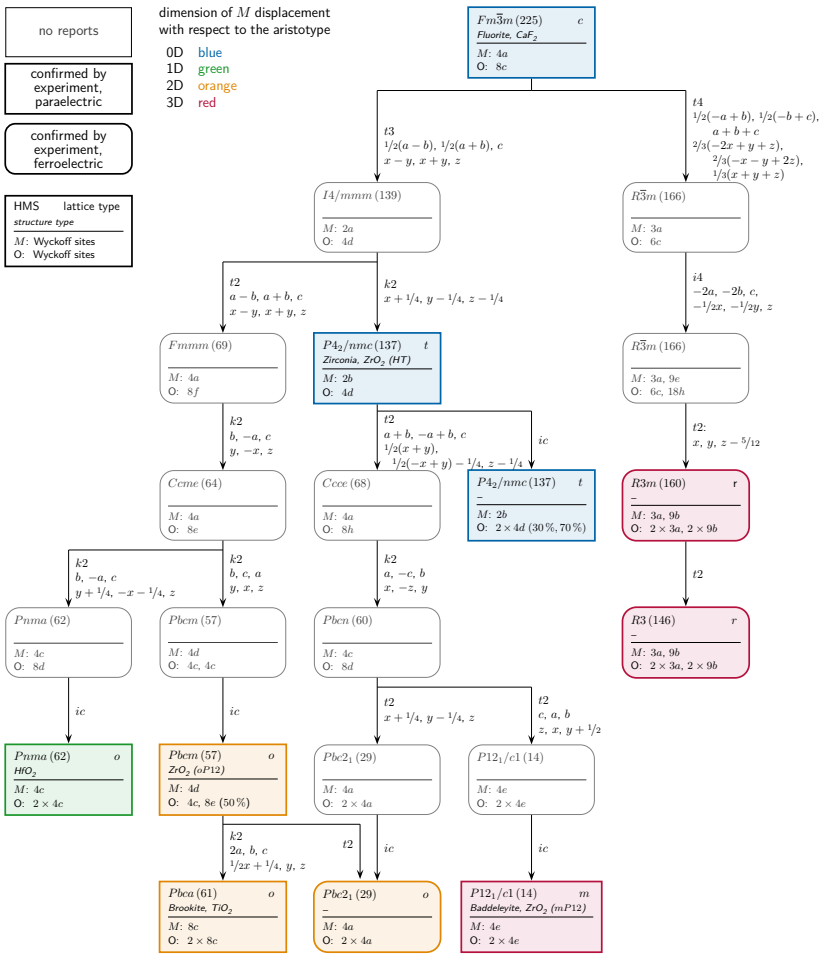

Fig. 1: Bärnighausen diagram of all experimentally reported $Hf_xZr_{1-x}O_2$ phases listed in the ICSD [15]. Each box represents a structure type within the $Hf_xZr_{1-x}O_2$ phases. The header includes the space group's Hermann-Mauguin number and symbol, the symbol of the lattice type (c – cubic, t – tetragonal, r – rhombohedral, o – orthorhombic, m – monoclinic, a – triclinic) and the official name of the structure type. The body presents the Wyckoff sites of the elements and their site occupancy factors, if applicable. A colorless box represents an auxiliary structure type that has no experimental evidence, but is essential to complete the diagram. A colored box represents eperimentally confirmed structure types; rounded corners indicate a ferroelectric structure type. The edge and filling of the box color-code the dimension of the M displacements with respect to the aristotype. Two boxes are interconnected with an arrow if they are direct group/subgroup pairs. The arrow's label includes the index and kind of transition (t – translationengleich, k – klassengleich, i – isomorph, ic – incoherent) as well as the transformations of the lattice (lattice vectors a, b, c and atomic coordinates x, y, z).

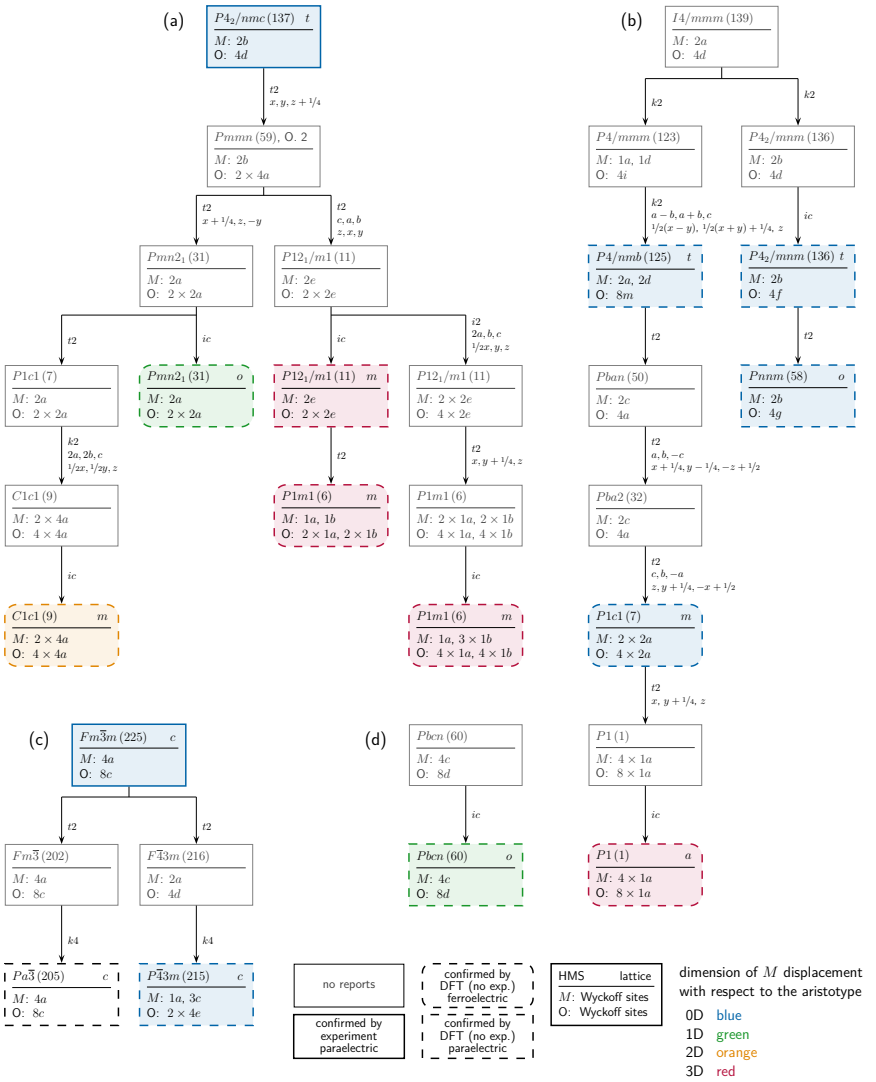

Fig. 2: Extension of the Bärnighausen diagram for the 13 structure types that are predicted by DFT (dashed frames) [10, 11]. The individual branches each base on a structure type that already exists in the experimental Bärnighausen diagram of Fig. 1 and represent (a) mainly monoclinic, (b) mainly tetragonal, (c) cubic, and (d) mainly orthorhombic types. See Fig. 1 for more details on the used symbols.

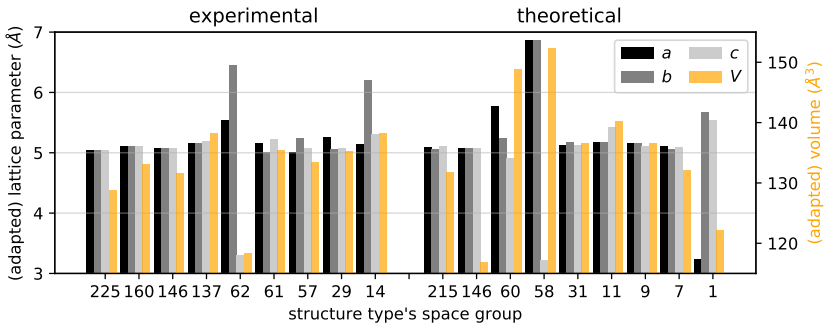

Fig. 3: Comparison of the atomic distances within the different structure types.
To compare the distances of the M atoms between the different structure types, mostly their lattice parameters can be utilized. The other types need to be transfered in a pseudo-cubic setting, *e. g.* the rhombohedral structure types (marked with star). The given volume corresponds to the given, adapted lattice parameters and the correct angles of this type. For experimentally confirmed strucutre types, the average of all literature values is presented.

3.1 Description of geometrical differences between the structure types

The differences between the vast amount of structure types can either be categorized by the branches in the Bärnighausen diagram or by the dimensionality of the displacements. The second approach is more efficient, as the focus lies on confirmed structure types while neglecting auxiliary structures to a reasonable extent and the geometrical differences are directly compared. Additionally, the geometrical description can be simplified by comparing all displacements to the aristotype. Further, the representation of the Bärnighausen diagram is not necessarily unique.

The following categorization primarily distinguishes between the displacements of the M atoms. These heavy atoms can be displaced in zero to three dimensions, relative to the aristotype in space group $Fm\bar{3}m$ (225). To simplify this comparison, the structures in the upcoming Fig. 5 to Fig. 9 were adapted in such a way, that the average distances of the M sublattice are identical to the aristotype, *i. e.* the lattice parameters are reshaped. The differences in lattice between the simplification and reality are discussed in an additional step using the visualisation of lattice parameters in Fig. 3. Next, the displacements of the O atoms are considered. Further, the group-subgroup path from the aristotype is briefly described. A subsequent section will discuss the set of structure types with severely tilted lattices, which cannot be compared visually to the aristotype anymore.

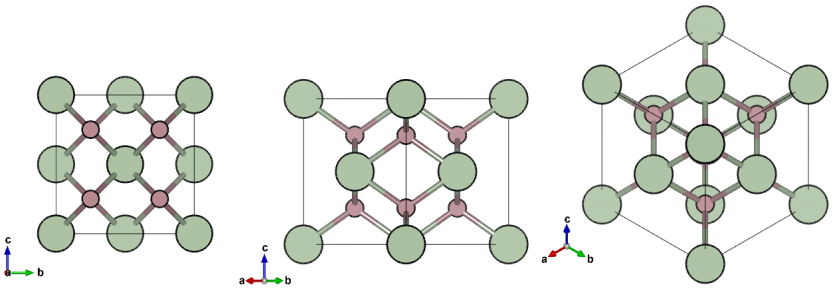

(a) [0 0 1] direction (b) [0 1 1] direction (c) [1 1 1] direction

Fig. 4: Different perspectives of the structure of the aristotype phase with space group $Fm\overline{3}m$ (225).

3.1.1 The aristotype.

The aristotype within the $Hf_xZr_{1-x}O_2$ family is of Fluorite type with SG $Fm\overline{3}m$ (225). In this type, the M atoms are 8-fold coordinated in a cube of O atoms. The O atoms, on the other hand, are tetrahedrally coordinated by the M atoms, see Fig. 4. The projections in Fig. 4 (b) and (c) are commonly found as primary direction in some derivative structure types, *e. g.* with SG 137 and SG 146, respectively.

3.1.2 No displacement of the M atoms.

Starting from the aristotype, the smallest structural differences occur, when the M atoms are not displaced from their ideal positions, which is mainly the case, for the cubic and tetragonal structure types. One of them is the predicted, cubic type with space group $P\overline{4}3m$ (215) [10]. During the change from the aristotype, the lattice parameters remain unchanged. Thus, the M sublattice of both structures is identical, although the M site nominally splits. Hence, the symmetry reduction is only caused by the displacement of the O atoms, with the displacement vector now pointing along a room diagonal, thus maintaining the cubic structure, see Fig. 5 (a). The 2-step transition involves the reduction of the 4-fold rotation to $\overline{4}$ and the subsequent unfixing of the O atom's coordinates.

This cubic structure type was found in an extensive theoretical study with the aim to predict all stable $Hf_xZr_{1-x}O_2$ phases [10]. The resulting structures were presented from the view of DFT calculations, which means that the atomic coordinates are derivations from those of the aristotype (four M atoms and eight O atoms). We transformed those structures to the crystallogrpahic point of view

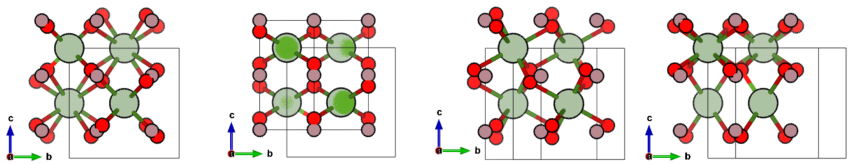

(a) $P\bar{4}3m\,(215)$ (b) $P4_2/nmc\,(137)$ (c) $P4_2/mnm\,(136)$ (d) $P4/nmb\,(125)$

Fig. 5: Overview over the different structure types without displacements of the M atoms. The aristotype is displayed in matte and the derivative in bright colours. The displacements are exaggerated for better visibility. The unit cell outline of the aristotype as well as of the strucutre of interest are given. The presented coordinate system belongs to the aristotype.

with FindSym [16, 17]. This step revealed that the refined atomic coordinates do not always fulfill the symmetric conditions of the SG within the given accuracy, but of a related SG with lower symmetry. In the case of SG 215, the transformation did not require any additional considerations, see Supplementary Material.

The second predicted cubic structure [10] has SG $Pa\bar{3}\,(205)$ and cannot be discussed here in detail, as the structure was classified as unstable and its structure parameters were not published. One possible GSR exists for a $t2$ followed by a $k4$ reduction as indicated in Fig. 2 (c). A subsequent *incoherent* transition cannot be excluded as it is required by most strucutre types within this family, see Supplementary Material.

The three tetragonal phases with SG 137, 136, and 125 differ in their dimension of the O displacements as well as in the volume change compared to the aristotype. The M distances of the high temperature Zirconia type with SG $P4_2/nmc\,(137)$ are larger than those of the aristotype, especially in the original c direction, which causes the reduction to the tetragonal lattice. The 1D displacement of the O atoms also points along the c direction, up- and downwards in a checkerboard pattern within the a, b plane, see Fig. 5 (b). The tranisition from the aristotype requires an intermediate reduction to SG $I4/mmm\,(139)$ and is caused by a rotation of the lattice by 45°, thus changing from face (F) to internally centred (I), which introduces is accompanied by a halving of the unit cell. A subsequent shift of the O atoms along the c direction leads to a transition to the Zirconia type, reducing the 4-fold rotation to the screw axis 4_2. Both structure types with SG 137 and 139 are each starting points for a branch of further structures, see Fig. 1 and Fig. 2 (a), (b).

As briefly mentioned, a disordered variant of the structure type with SG 137 has also been reported [18]. In this variant, about 70 % of the O atoms remain at their high symmeric position, while the others are displaced from it. This partial displacement results in a split into two independent, not fully occupied Wyckoff sites. The corresponding transition cannot be expressed with GSR, because the

involved SGs are identical and would thus require an *isomorphous* transition. As the cell size does not change, the transition would be of index 1. However, an *isomorphous* transition of index 1 is an identical mapping, which contradicts the split of the O position. Though, the partially disordered structure could also be the misinterpretation of a twin, espeically because only one author described it. Whatsmore, when combining only one of the O sites with the M position, both combinations result in reasonable, individual descriptions of the Zirconia type with an O displacement of 0.00 or 0.09, respectively, compared to an average of 0.048 of all Zirconia compounds within the $Hf_xZr_{1-x}O_2$ family.

Another predicted structure type nominally has the SG $P4_2/mnm$ (136) [10]. In this type, the O atoms are systematically displaced by $1/8$ or $3/8$ in a and b direction of the new cell, see Fig. 5 (c). Now, some of the O atoms are located at the area diagonal of the a, b plane between the M atoms. Thus, the in-plane $M-M$ distances are strongly enhanced, while the out-of plane distances are slightly shortened. The transition from SG 139 displayed in Fig. 2 (b) involving an *incoherent* transition describing the aforementioned severe O displacements. The details of the *incoherent* transition are explained in the Supplementary Material. The presented lattice of this predicted structure [10] was inadequate and, especially, the given atomic coordinates only fulfilled the conditions of SG $Pnnm$ (58), but not for the given, higher symmetric SG 136. Therefore, we additionally present this type in SG 58 with the dedicated symmetry reduction.

The last structure type without displacement of the M atoms is the predicted tetragonal structure [10] with SG $P4/nmb$ (125). Here, the lattice parameters remain unchagned with respect to the aristotype, hence, the symmetry reduction is solely caused by the displacement of the O atoms. In contrast to the structure type with SG 137, the O displacements are mainly pointing along the area diagonal of the b, c plane and not along c. As a result, the structure consists of two consecutive M planes with tighter and looser coordination, respectively, see Fig. 5 (d). The transition is again based on SG 139, starting with a reduction to a primitive cell (P) with SG 123, see Fig. 2 (b). Subsequently, a lattice rotation by 45° is accompanied with the split of the M position. The structure type with SG 125 was presented by Barabash [10], however the given structural parameters suite to SG $P1c1$ (7). The symmetry reduction from SG 125 to SG 7 involves reductions of a 4-fold rotation and a glide plane.

3.1.3 1D displacement of the M atoms.

The structure types with M being displaced in 1D have orthorhombic lattices with SGs $Pbcn$ (60), $Pnma$ (62) and $Pmn2_1$ (31). In all cases, the O atoms are displaced

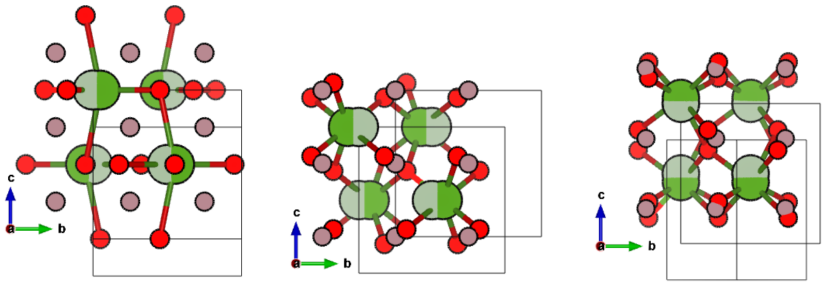

(a) *Pnma* (62) (b) *Pbcn* (60) (c) $Pmn2_1$ (31)

Fig. 6: Overview over the different structure types with a 1D displacements of the M atoms. The aristotype is displayed in matte and the derivative in bright colours. The displacements are exaggerated for better visibility. The unit cell outline of the aristotype as well as of the strucutre of interest are given. The presented coordinate system belongs to the aristotype.

in 3D. The M displacement of the Hafnia structure type with SG *Pnma* (62) is along the y direction. This type shows the strongest compression along the c direction among the experimentally confirmed types, see Fig. 3. The cause for this compression is the movement of the M atoms along the b direction, such that atoms with the same a component shift in the same direction, whereas the sign changes for adjacent atoms. These displacements are accompanied by a lattice stretch in b direction. In turn, this stretch gives the atoms more space, which can be compensated for with the compression in c direction. At the same time, the O atoms are severely shifted, consequently they are now located within the same a, b plane as the M atoms and the position splits into two, see Fig. 6 (a). The transition from SG 139 to *Pnma* (62) requires several intermediate steps starting with the loss of the 4-fold rotation symmetry resulting in a rotation of the lattice to the orthorhrombic SG *Fmmm* (69). Subsequently, the O atom gains an additional degree of freedom, accompanied with the reduction of two mirrors into glide planes during a transition to SG *Ccme* (64), see Fig. 1. Further, the double glide plane is reduced to a diagonal glide plane to reach SG 62, see Supplementary Material.

The second orthorhombic type with 1D M displacement is the theoretically predicted [10] type with SG *Pbcn* (60). Here, the movements of the M atoms have a different character. All M atoms within one c layer move towards the same direction in b, the sign changes between adjacent c layers, see Fig. 6 (b). Additionally, the O atoms are only slightly displaced, but in all directions, without forcing a split position. Further, lattice parameter b is strongly elongated, see Fig. 3. This structure type can be derived from SG 137 with an auxiliary step over SG *Ccce* (68), see Fig. 1 and Fig. 2 (d). The details of the *incoherent* transition

are explained in the Supplementary Material. The auxiliary structure type with SG 68 has been experimentally reported once [19, 20]. However, the same structure description can already be realized with the higher symmetric SG 137.

The M atoms of the structure type with SG $Pmn2_1$ (31) are displaced along the c direction, see Fig. 6 (c). In this predicted structure [11], one c layer is positively displaced, while the adjacent layers are negatively displaced, see Fig. 6 (c). Additionally, the O atoms are shifted in 3D along the a, b in-plane diagonal, with an additional smaller c component; again without causing a split position. The atomic arrangement is only slightly distorted, the interatomic distances and the volume hardly change. The structure type can be derived from SG 137 via the intermediate SG $Pmmn$ (59), see Fig. 2 (a), losing the 4-fold rotational symmetry and a mirror. Additionally, an *incoherent* transition must be noted, see Supplementary Material.

3.1.4 2D displacement of the M atoms.

Three structure types exhibit a 2D displacement of the M atoms, all of them are orthorhombic with a displacement within the a, b plane, see Fig. 7. The two orthorhombic structure types with SGs $Pbcm$ (57) and $Pbc2_1$ (29), respectively, exhibit a split of the O position. Additionally, for both, the cell dimensions remain almost identical to those of the aristotype, with only a slight enlargement of the b parameter, see Fig. 3. In the former structure type, the O atoms are displaced in 1D and 3D, whereas 2D and 3D displacements occur for the latter type. This small difference is the origin of the ferroelectricity of the structure type with SG $Pbc2_1$ (29).

In the higher symmetric structure type with SG $Pbcm$ (57), one of the O sites has a doubled Wyckoff index with halved occupation, see Fig. 7 (a)–(c). The transition from SG 64 requires a transition to an intermediate SG 57 reducing a mirror to a glide plane, see Fig. 1. For the experimentally confirmed structure type with SG 57, an additional *incoherent* transition is required to realize the aforementioned doubled Wyckoff index, see Supplementary Material.

The lower symmetric type with SG $Pbc2_1$ (29) can be regarded as an ordered variant, but with additional degrees of freedom for the displacement in b direction due to the loss of inversion symmetry. The relation is emphasized in Fig. 8 and Tab. 1. In SG 57, the atoms with labels 0/1, 2/3, 4/5, 6/7 form couples, from which always that atom with lower c value is fully occupied in SG 29, the other is not occupied at all. This structure type can be derived in several ways from the existing paths in the Bärnighausen diagram. Two of them are displayed in Fig. 1. The first one is the traditional way already described by [21] via SG 60. The second one uses the intended relation to SG 57.

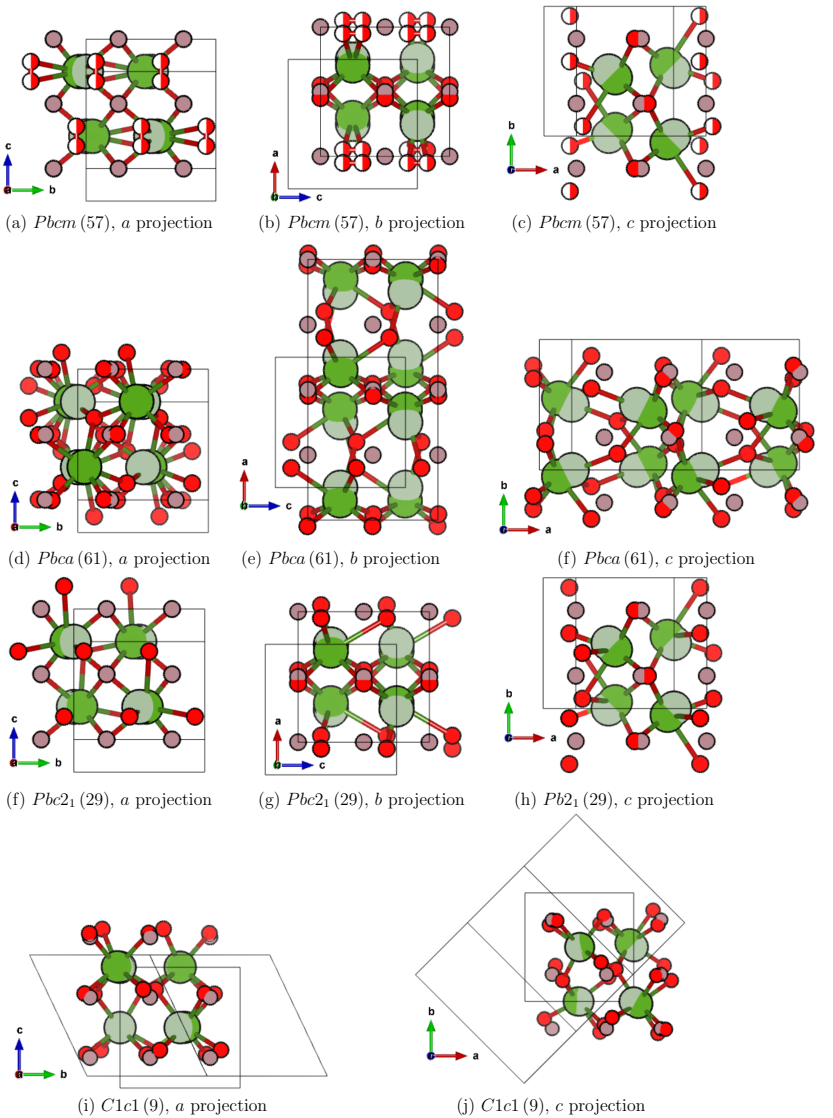

(a) *Pbcm* (57), *a* projection (b) *Pbcm* (57), *b* projection (c) *Pbcm* (57), *c* projection

(d) *Pbca* (61), *a* projection (e) *Pbca* (61), *b* projection (f) *Pbca* (61), *c* projection

(f) $Pbc2_1$ (29), *a* projection (g) $Pbc2_1$ (29), *b* projection (h) $Pb2_1$ (29), *c* projection

(i) *C*1*c*1 (9), *a* projection (j) *C*1*c*1 (9), *c* projection

Fig. 7: Overview over the different structure types with a 2D displacements of the M atoms. The aristotype is displayed in matte and the derivative in bright colours. The displacements are exaggerated for better visibility. The unit cell outline of the aristotype as well as of the strucutre of interest are given. The presented coordinate system belongs to the aristotype.

Tab. 1: Visualisation of the ordering of the Zirconia $oP12$ type with SG $Pbcm\,(57)$ resulting in the ferroelectric type with SG $Pbc2_1\,(29)$ or in the monoclinic type with SG $P12_1/c1\,(14)$. The given coordinates originate from the ICSD data sets 53034, 67004, and 60903 for SG 57, 29, and 14, respectively. The transition is retracable in the Bärnighausen diagram Fig. 1. The labels of SG 57 correspond to the ones in Fig. 8.

	$Pbcm\,(57)$					$Pbc2_1\,(29)$				$P12_11\,(14)$			
	site	a/x	b/y	c/z	**label**	**site**	a/x	b/y	c/z	**site**	a/x	b/y	c/z
Hf	$4d$	0.26	0.03	1/4		$4a$	0.27	0.03	0.25	$4e$	0.28	0.04	0.21
		0.74	0.97	3/4			0.73	0.97	0.75		0.72	0.96	0.79
		0.74	0.53	1/4			0.73	0.53	0.25		0.72	0.54	0.29
		0.26	0.47	3/4			0.27	0.47	0.75		0.28	0.46	0.71
O	$4c$	0.54	1/4	0	**10**	$4a$	0.54	0.23	0	$4e$	0.55	0.26	0.02
		0.46	3/4	1/2	**9**		0.46	0.77	0.5		0.45	0.76	0.48
		0.46	3/4	0	**11**		0.46	0.73	0		0.45	0.74	0.98
		0.54	1/4	1/2	**8**		0.54	0.27	0.5		0.55	0.24	0.52
O	$8e$	0.08	0.375	0.13	**5**	$4a$	0.07	0.36	0.11	$4e$			
		0.92	0.625	0.63	**3**		0.93	0.64	0.61		0.93	0.67	0.65
		0.92	0.875	0.37	**6**								
		0.08	0.125	0.87	**0**						0.07	0.17	0.85
		0.92	0.625	0.87	**2**								
		0.08	0.375	0.37	**4**						0.07	0.33	0.35
		0.08	0.125	0.63	**1**		0.07	0.14	0.61				
		0.92	0.875	0.13	**7**		0.93	0.86	0.11		0.93	0.83	0.15

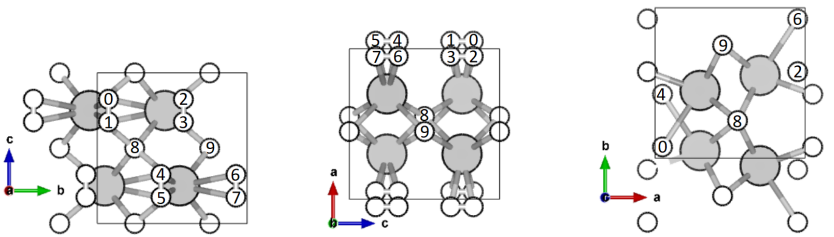

(a) a projection (b) b projection (c) c projection

Fig. 8: Schematic view on the similarities between the SGs 57, 61, 29, and 14.

In the Brookite type with SG *Pbca* (61), all M atoms within one c layer have the same y displacement and the sign of the x displacement changes between adjacent lines with the same y component, see Fig. 7 (d)–(f). For adjacent c layers the signs of the x and y displacements change. The O site is split to four positions. Two of the sites are 2D, the other two are 3D displaced. The 2D displacements affect the same O position of adjacent cells along a direction with opposite displacements of the y component. The same applies to the 3D displacements. Therefore, the cell doubles along a direction with respect to the aristotype. Beside the nominally doubled cell in a, the interatomic distances are elongated along b. The transition to SG 61 can be realized in this Bärnighausen tree in two different ways. First, by a $k2$ transition that depicts the reduction of a mirror to a glide plane. The required doubling of the cell cannot be realized by a transition between SG 64 to 61, nor by an *isomorphic* transition of SG 61. Thus, an *incoherent* transition is required here, additionally involving severe displacements of one of the O sites from their previous positions, see Supplementary Material. Second, the Brookite type is directly related to the experimentally confirmed Zirconia $oP12$ type with SG 57. In both types, the M site and one of the O sites are identical regarding symmetry and coordination when comparing cells with identical sizes, see the two upper blocks in Tab. 2 and Fig. 7 (a)–(c). The remaining O site can be regarded as frozen disorder as briefly mentioned in [19]: the atomic coordinates are identical, but the occupation is reduced in SG *Pbcm* (57), lower block in Tab. 2. Figure 7 reveals that the O atoms in the first half of the super cell occupy the positions 0, 2, 4, and 6, whereas in the second half, the O atoms occupy the complementary positions 1, 3, 5, and 7, compare with Fig. 8.

The last structure type with 2D displaced M atoms is the predicted type with SG $C1c1$ (9) [11], which can be derived from SG 31. This type is one of the rare cases with a split M site, from which one is displaced in 1D, the other in 2D; the c component is unaffected by the displacements. Additionally, the O atoms are split onto four sites, all displaced with the same sign along the c direction. Consequently, the M atoms are no longer at the approximate center of their coordinating O atoms, making the structure ferroelectric. Additionally, the lattice is tilted with $\beta \approx 120°$. Simultaneously, the cell is doubled in b direction and the interatomic distances are slightly enlarged, especially in b and c direction.

3.1.5 3D displacement of the M atoms.

In total, three structure types exist, in which the M atoms are displaced in 3D while leaving the overall lattice comparable to the aristotype. One of them has the rhombohedral SG $R3$ (146), see Fig. 9 (a)-(c). Here, the M displacements lead

Tab. 2: Visualisation of the partial ordering of the Brookite type with SG $Pbca\,(61)$ resulting in the Zirconia $oP12$ type with SG $Pbcm\,(57)$. The transition is retracable from the Bärnighausen diagram Fig. 1 and involves the shift of the origin in a direction and a subsequent doubling of the x coordinate as indicated in the 2nd column. Associated M positions are indicated with a superscripted lettre and O atoms via label. The given coordinates originate from the ICSD data sets 53034 and 173960 for SG 57 and 61, respectively.

	$Pbca\,(61)$				**adaption SG 61** $2(x+1/4), y, z$			$Pbcm\,(57)$				
	site	a/x	b/y	c/z	a/x	b/y	c/z	**site**	a/x	b/y	c/z	**label**
Hf	$8c$	0.89	0.04	0.26	0.28	0.04	0.26^a	$4d$	0.26	0.03	$1/4^a$	
		0.61	0.96	0.76	0.72	0.96	0.76^b		0.74	0.97	$3/4^b$	
		0.11	0.54	0.24	0.72	0.54	0.24^c		0.74	0.53	$1/4^c$	
		0.39	0.46	0.74	0.28	0.46	0.74^d		0.26	0.47	$3/4^d$	
		0.11	0.96	0.74	0.72	0.96	0.74^b					
		0.39	0.04	0.24	0.28	0.04	0.24^a					
		0.89	0.46	0.76	0.28	0.46	0.76^d					
		0.61	0.54	0.26	0.72	0.54	0.26^c					
O	$8c$	0.98	0.74	0.49	0.46	0.74	0.49	$4c$	0.46	3/4	1/2	**9**
		0.52	0.26	0.99	0.54	0.26	0.99		0.54	1/4	0	**10**
		0.02	0.24	0.01	0.54	0.24	0.01					**10**
		0.48	0.76	0.51	0.46	0.76	0.51					**9**
		0.02	0.26	0.51	0.54	0.26	0.51		0.54	1/4	1/2	**8**
		0.48	0.74	0.01	0.46	0.74	0.01		0.46	3/4	0	**11**
		0.98	0.76	0.99	0.46	0.76	0.99					**11**
		0.52	0.24	0.49	0.54	0.24	0.49					**8**
O	$8c$	0.79	0.375	0.13	0.08	0.375	0.13	$8e$	0.08	0.375	0.13	**5**
		0.71	0.625	0.63	0.92	0.625	0.63		0.92	0.625	0.63	**3**
		0.21	0.875	0.37	0.92	0.875	0.37		0.92	0.875	0.37	**6**
		0.29	0.125	0.87	0.08	0.125	0.87		0.08	0.125	0.87	**0**
		0.21	0.625	0.87	0.92	0.625	0.87		0.92	0.625	0.87	**2**
		0.29	0.375	0.37	0.08	0.375	0.37		0.08	0.375	0.37	**4**
		0.79	0.125	0.63	0.08	0.125	0.63		0.08	0.125	0.63	**1**
		0.71	0.875	0.13	0.92	0.875	0.13		0.92	0.875	0.13	**7**

Tab. 3: Comparison of the two different structure solutions for the rhombohedral structure type with SG $R3\,(146)$ from experiment [2] and DFT calculations [10]. The structures had an offset in c direction relative to each other by 0.003 relative lattice units.

	DFT calculation $a = 7.174$ Å, $c = 9.088$ Å				**experiment** $a = 7.106$ Å, $c = 9.016$ Å			**abs. difference**		
M	$3a$	0.000	0.000	0.521	0.000	0.000	0.521	0.000	0.000	0.000
M	$9b$	0.327	0.136	0.206	0.327	0.191	0.206	0.000	−0.055	0.000
O	$3a$	0.000	0.000	0.291	0.000	0.000	0.291	0.000	0.000	0.000
O	$3a$	0.000	0.000	0.881	0.000	0.000	0.882	0.000	0.000	−0.001
O	$9b$	0.191	0.323	0.115	0.133	0.323	0.115	0.058	0.000	0.000
O	$9b$	0.066	0.485	0.314	0.066	0.579	0.314	0.000	−0.094	0.000

to a two-fold split of the position. Additionally, the O atoms are now located on four Wyckoff sites, which are 2D and 3D displaced, causing ferroelectricity in the material. The interatomic distances are slightly enlarged in all dimensions. The transition takes place in three steps. A first auxiliary step allows a movement of the O atom along the space diagonal, which leads to the transition to SG $R\bar{3}m\,(166)$. Further, the decoupling of the atomic sites and the doubling of the unit cell in a and b direction takes place via an $i4$ transition. Subsequently, the transition to SG $R3m\,(160)$ realizes the free atomic coordinates of the M atoms. In this structure type, x and y coordinates are still coupled to each other; the decoupling is described by a further *translationengleich* transition to SG $R3\,(146)$. This structure type was first predicted in 2017 [10]. One year later, a thin film was grown, reportedly with its structure in SG 146 or 160 [2], which was not uniquely identifiable. The comparison of both structure refinements shows that all $3a$ sites of the structures are identical to each other. Only the $9b$ sites differ from each other by less than 10 %, see Tab. 3. The lattice parameters are even more accurate with less then 1 % deviation. In summary, the real structure was very accurately predicted by theory.

Another structure with 3D displaced M atoms is the well known monoclinic phase Baddeleyite with SG $P12_1/c1\,(14)$. The O atoms are located on two sites, both displaced in 3D, accompanied with an increase of the β angle to 99.0° (averaged over all available literature values). This phase is again highly similar to the aforementioned orthorhombic phases, especially to the Zircona $oP12$ type and the ferroelectric type with SG $Pca2_1\,(29)$, compare Fig. 9 (d)-(f) with Fig. 8. Baddeleyite is another ordered variant of the Zirconia $oP12$ type, similar to the ferroelectric, orthorhombic phase, but with a different selection of atomic coordinates of the second O atom, see Tab. 1. In contrast to the ferroelectric type, the atoms are shifted in such a way that the lattice is not cartesian anymore due to the increase of β. Again, an *incoherent* transition is involved, which only affects

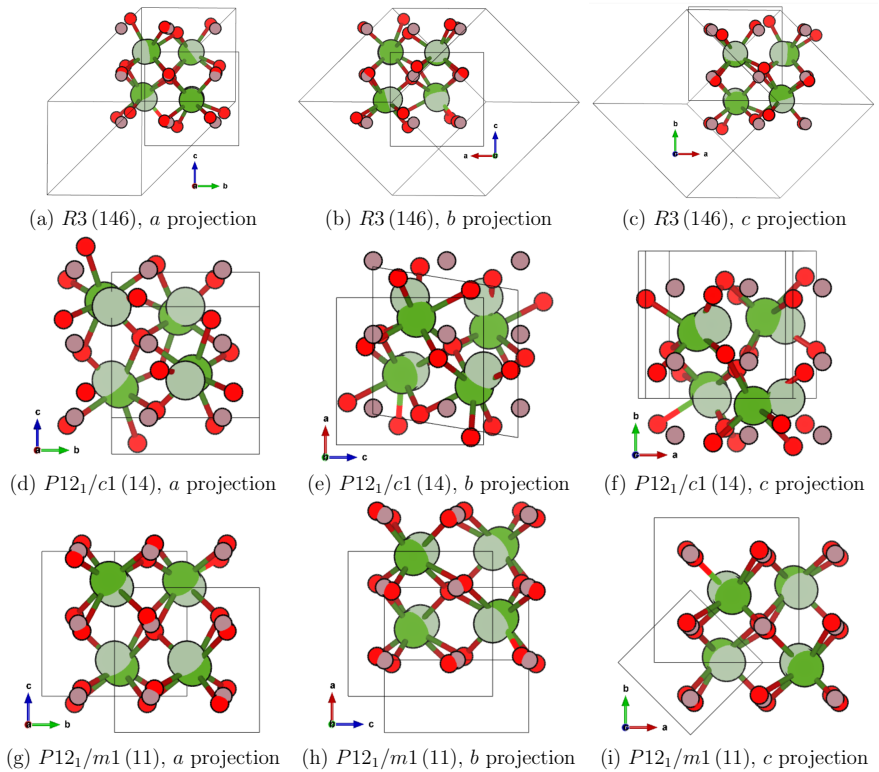

(a) $R3\,(146)$, a projection (b) $R3\,(146)$, b projection (c) $R3\,(146)$, c projection

(d) $P12_1/c1\,(14)$, a projection (e) $P12_1/c1\,(14)$, b projection (f) $P12_1/c1\,(14)$, c projection

(g) $P12_1/m1\,(11)$, a projection (h) $P12_1/m1\,(11)$, b projection (i) $P12_1/m1\,(11)$, c projection

Fig. 9: Overview over the different structure types with 3D displacements of the M atoms, without lattice distortions. The aristotype is displayed in matte and the derivative in bright colours.

the second O site, see the Supplementary Material. This transition was already discussed by [21], who found in total ten transition paths. However, they did not check those paths for valid transformations of the lattice, the Wyckoff positions and atomic coordinates. In fact, only the five paths via SG *Ccce* (68) involve a rotation of the lattice by 45° as the structure types require. All other paths can be excluded. Further, the descent from SG 68 to SG 13 involves a tilt of the lattice, which also does not describe the desired relation. All four remaining paths are valid and display the occupational ordering as described in Fig. 8. Here, the positions with labels 0/1 and 6/7 form couples, from which the atom with lower c value is occupied. From the couples 2/3 and 4/5, the position with higher c value is occupied.

The last structure type with 3D displaced M atoms is the predicted, monoclinic type with SG $P12_1/m1$ (11) [10], which has a split O site. The displacements cause a rotation of the lattice by 45° accompanied with halving the cell. The interatomic distances are enlarged with respect to the aristotype, especially in c direction, see Fig. 3. The symmetry reduction involves a further *incoherent* transition to describe the atomic positions of the theoretical reported structure type in the correct way, see Fig. 2 (a). However, similar to the inaccurate data of SG 215 and 136, the details given on the relaxed structure categorized with SG 11, are in fact matching with SG 6. The symmetry reduction involves the loss of the screw axis.

3.1.6 3D displacement of the M atoms accompanied with distorted lattices.

The most severe distortions occur for structure types with 3D displaced M atoms accompanied with a severely distorted lattice. All affected structure types are predicted with DFT, without experimental reports. An adequate visual presentation is challenging because the aristoypic structure cannot be recognized in the derivative. Therefore, only the structure types themselves are depicted and the aristotype is omitted in Fig. 10.

The structure type with SG $P1m1$ (6) and twelve atoms in the unit cell was predicted by DFT [11]. This structure type is not related with the previously mentioned type with only six atoms in the until cell: the pseudo-cubic sublattice of the M atoms is lost, see Fig. 2 (a). In this type, β equals 84°, still the b projection has a strong resemblance to the previously described structure types, see Fig. 10 (b). However, the two other projections hardly resemble the aristotype.

Finally, a complete loss of symmetry was predicted to be stable [11]. In the triclinic structure type with SG $P1$ (1) the M and O atoms are split in four and eight sites, respectively. Remarkably, one of the M atoms is strongly displaced across half of the aristotype's unit cell along a direction. Additionally, two O

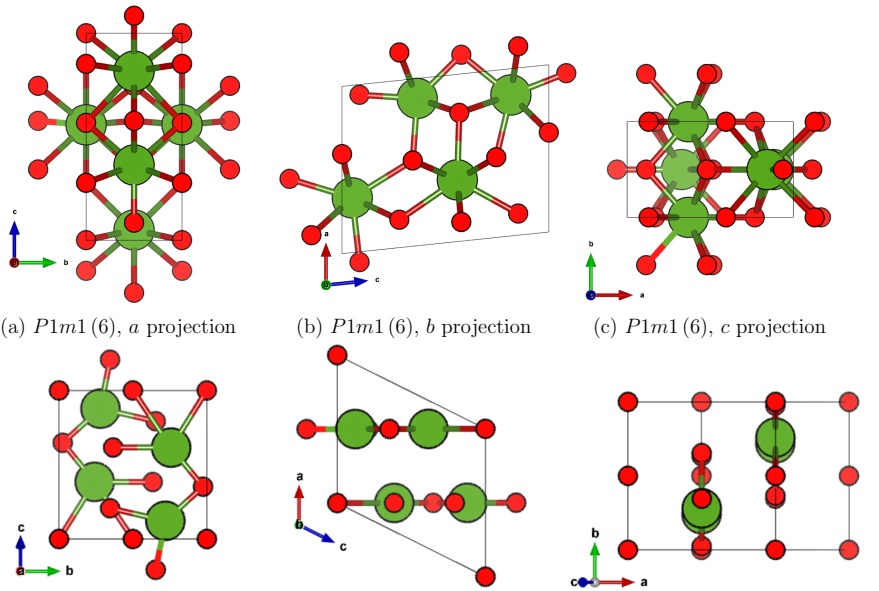

(a) $P1m1\,(6)$, a projection (b) $P1m1\,(6)$, b projection (c) $P1m1\,(6)$, c projection

(d) $P1\,(1)$, a projection (e) $P1\,(1)$, b projection (f) $P1\,(1)$, c projection

Fig. 10: Overview over the different structure types with a 3D displacements of the M atoms, accompanied with a distortion of the lattice. The presentation of the aristotype is omitted because of too great differences.

atoms are shifted about $^1/_4\,c$ and now occupy the location where the severely shifted M atom was before. Those displacements cause some kind of shearing of the M layers along a direction, causing an enlargement of β to $\approx 104°$ and also a strong compression along b. The volume is maintained with regard to the aristotype. For example, the transition path can be realized starting from SG 7, involving an *incoherent* transition, see Fig. 2 (c).

3.2 Possible Applications

Now that we have constructed the Bärnighausen trees and the transition paths are known, a more specific analysis is possible. The knowledge of the geometrical changes during the GSR allows conclusions on appearing and disappearing reflections during the phase transition. Thus, a detailed, experimental characterization of the phase transition, *e. g.* its dynamics, is now possible.

For each group-subgroup transition, the change of the lattice vectors is given in the labels at the arrows. Further, a vector in real space accords to a point in reciprocal space. Therefore, by knowing the relation of the lattice vectors between two group-subgroup related SGs, we also know the relation of the reflections. In conclusion, we can now assign the reflections of those structure types in regard to each other and calculate systematically their existance and, whatsmore, their intensity in both phases. This assignment now allows *e. g.* the characterization of phase transitions *in-situ* [22, 9] or the selection and analysis of reflections that are sensitive on polarization changes with resonant X-ray methods like *Resonantly Suppressed Diffraction* (RSD) [23]. We will now discuss this approach for two examples of the $Hf_xZr_{1-x}O_2$ family.

3.2.1 Transition from the ferroelectric, orthorhombic to the tetragonal phase.

The phase transition from the ferroelectric, orthorhombic structure type with SG $Pbc2_1$ (29) to the tetragonal type with SG $P4_2/nmc$ (137) at approximately 450 °C is well known [22]. A detailed analysis of this phase transition was reported for the 1 1 0 reflection [22, 9]. Further reflections were not considered so far. However, 1 1 0 cannot be the only sensitive reflection.

To find all these reflections, the lattice vector transition between start and end phase needs to be constructed. Afterwards, for each reflection from the start phase, the corresponding reflection of the end phase is calculated and both are evaluated regarding their reflection conditions.

As the transition occurs from the orthorhombic to the tetragonal phase with increasing temperature, we define $Pbc2_1$ (29) to be the start point and $P4_2/nmc$ (137) as the end point. The group-subroup path is not unique and can either go via SG 68 or 64. The shorter and more intuitive way is the former one as it does not involve an ascending step to SG 139. This path includes two steps with changing lattice vectors, combining to the following transition matrix:

$$M_{68\to60} \cdot M_{137\to68} = M_{\text{total}}$$
$$\begin{pmatrix} 1 & 0 & 0 \\ 0 & 0 & -1 \\ 0 & 1 & 0 \end{pmatrix} \cdot \begin{pmatrix} 1 & 1 & 0 \\ -1 & 1 & 0 \\ 0 & 0 & 1 \end{pmatrix} = \begin{pmatrix} 1 & 1 & 0 \\ 0 & 0 & -1 \\ -1 & 1 & 0 \end{pmatrix}.$$

As the step from SG 29 to 60 does not involve a lattice transformation, the matrix $M_{68\to60}$ is equivalent with $M_{68\to29}$. Thus, M_{total} gives the transition from a reflection R_{137} of the structure type in SG 137 to a reflection R_{29} of the structure type in SG 29. By inversion of the matrix M_{total}, a reflection of SG 29 can be transformed into a reflection of SG 137:

$$R_{137} = M_{\text{total}}^{-1} \cdot R_{29}.$$

Now that the reflections can be assigned to each other, the next step is to identify those, that are allowed in only one of both phases. We evaluated all 8000 reflections of the orthorhombic phase in the range -10 to 9 for all Miller indices h, k, l. From those, 110 are forbidden in both, 7310 are allowed in both, 290 are allowed in the orhtorhombic phase, but forbidden in the tetragonal phase and 290 are allowed in the tetragonal phase, but forbidden in the orthorhombic one.

To follow the temperature dependent transition during a measurement, starting with an allowed reflection is most reasonable. Now, the conditions to the reflections can be narrowed, *e. g.* the reflection is in the Ewald sphere of the chosen energy, the intensity is sufficiently high when starting and the angle between reflection and surface is adequate for the setup. All those considerations can be evaluated using the pyasf module [24]. For an evaluation at the Hf L_3 absorption edge at 9.56 keV, the above considerations return those reflections with $l = 0$ and k odd.

3.2.2 Transition from the ferroelectric, rhombohedral to the cubic phase.

A similar intellectual game exists for the ferroelectric rhombohedral phase with SG $R3$ (146). This phase is expected to have a phase transition at high temperatures ($\approx 700\,^{\circ}\text{C}$) towards the cubic phase with SG $Fm\overline{3}m$ (225). The transition includes

two steps affecting the lattice vectors. However, the *isomorphous* transition between the quadrupled and single cell in SG 166 does not affect the Miller indexing. Thus, the geometric transition is described by

$$M_{225\to166} = M_{\text{total}} = \begin{pmatrix} -1/2 & 1/2 & 0 \\ 0 & -1/2 & 1/2 \\ 1 & 1 & 1 \end{pmatrix}.$$

The matrix M_{total} gives the transition from a reflection R_{225} to a reflection R_{146}, corresponding to the structure types in SG 225 and 146, respectively.

Again, all 8000 reflections of the start phase in the range -10 to 9 for all Miller indices are analyzed, however this time, the start phase is rhombohedral. From those, all are allowed in the cubic phase; 2667 reflections are also allowed in the rhombohedral phase, while the other 5333 are forbidden. Therefore, the analysis of this phase transition will be experimentally more challenging as only additional reflections appear during heating, but none disappear, which implies the unfortunate case to start a measurement at a spot with zero intensity at room temperature.

Assuming a $[0, 0, 1]$ surface of the rhombohedral phase [2], the most promising reflections for this experiment are $0\,0\,l$ with an even l.

4 Conclusion

In the present work, we acquired a comprising overview of the great diversity in crystal strucutres within the $Hf_xZr_{1-x}O_2$ family. Precisely because of this diversity, we strongly recommend to always clarify, which structure type is referred to by specifying the according SG. Further, we displayed the symmetric relations between the structure types that are often very close to each other, indicating possible simple phase transitions between them. Especially for the three orthorhombic types with SGs 57, 61, 29 and the monoclinic type with SG 14, a simple phase transition could be possible as those phases are directly related.

Additionally, by knowing the transition paths, reflections of phases that are related to each other by phase transitions can be converted into each other. This technique is not only applicable for the $Hf_xZr_{1-x}O_2$ family but is universal. This approach allows to choose suitable reflections to investigate phase transitions and evaluate them in terms of different characteristics, *e. g.* slope of intensity (rapidness of transition) as in [22].

Further, the analysis of the structural differences between the phases regarding atomic positions and especially the lattice, could give insights to necessary growth

conditions for each individual phase in terms of adequate choice of the subsrate or potential use of doping atoms.

Acknowledgment: This project has received funding from the European Union's Horizon 2020 research and innovation programme under grant agreement No. 871072. The authors like to thank Beatrix Noheda for inspiring discussions.

References

[1] K. Uchino, *Ferroelectric Devices*. CRC Press, 2018. https://books.google.de/books?hl=de&lr=&id=5QvLBQAAQBAJ&oi=fnd&pg=PP1&dq=ferroelectric&ots=_c6JF2Xpdo&sig=odh-kp4jhjggfV4F9Maa8Ob_2s0#v=onepage&q=ferroelectric&f=false, p. 20.

[2] Y. Wei, P. Nukala, M. Salverda, S. Matzen, H. J. Zhao, J. Momand, A. S. Everhardt, G. Agnus, G. R. Blake, P. Lecoeur, J. Kooi, B. J. ande Íñiguez, B. Dkhil, and B. Noheda, "A rhombohedral ferroelectric phase in epitaxially strained $Hf_{0.5}Zr_{0.5}O_2$ thin films," *Nature Mater.*, vol. 17, p. 1095, 2018.

[3] Y. Li, R. Liang, J. Wang, Y. Zhang, H. Tian, H. Liu, S. Li, W. Mao, Y. Pang, Y. Li, Y. Yang, and T.-L. Ren, "A ferroelectric thin film transistor based on annealing-free HfZrO film," *IEEE Journal of the Electron Devices Society*, vol. 5, no. 5, p. 378, 2017.

[4] R.-W. Kao, H.-K. Peng, K.-Y. Chen, and Y.-H. Wu, "$HfZrO_x$-Based Switchable Diode for Logic-in-Memory Applications," *IEEE Transactions on Electron Devices*, vol. 68, no. 2, p. 545, 2021.

[5] M. Dragoman, M. Aldrigo, D. Dragoman, S. Iordanescu, A. Dienscu, and M. Modreanu, "HfO_2-Based Ferroelectrics Applications in Nanoelectronics," *Phys. Status Solidi*, vol. 15, p. 2000521, 2021.

[6] Z. Zheng, R. Cheng, Y. Qu, X. Yu, W. Liu, Z. Chen, B. Chen, Q. Sun, D. W. Zhang, and Y. Zhao, "Real-Time Polarization Switch Characterization of $HfZrO_4$ for Negative Capacitance Field-Effect Transistor Applications," *IEEE Electr. Device L.*, vol. 39, p. 1469, 2018.

[7] K. Z. Rushchanskii, S. Blügel, and M. Ležaić, "Ordering of oxygen vacancies and related ferroelectric properties in $HfO_{2-\delta}$," *Phys. Rev. Lett.*, vol. 127, p. 087602, 2021.

[8] M. H. Park, Y. H. Lee, H. J. Kim, Y. J. Kim, T. Moon, K. D. Kim, J. Müller, A. Kersch, U. Schroeder, T. Mikolajick, and C. S. Hwang, "Ferroelectricity and Antiferroelectricity of doped thin HfO_2-based films," *Adv. Mater.*, vol. 27, p. 1811, 2015.

[9] T. Mimura, T. Shimizu, O. Sakata, and H. Funakubo, "Large thermal hysteresis of ferroelectric transition in HfO_2-based ferroelectric films," *Appl. Phys. Lett.*, vol. 118, p. 112903, 2021.

[10] S. V. Barabash, "Prediction of new metastable HfO_2 phases: toward understanding ferro- and antiferroelectric films," *J. Comput. Electron.*, vol. 16, p. 1227, 2017.

[11] T. D. Huan, V. Sharma, G. A. Rossetti, and R. Ramprasad, "Pathways towards ferroelectricity in hafnia," *Phys. Rev. B*, vol. 90, p. 064111, 2014.

[12] T. Hahn, ed., *International tables for crystallography*, vol. A. Kluwer, 2006.

[13] H. Wondraschek and U. Müller, eds., *International tables for crystallography*, vol. A1. Kluwer, 2006.

[14] G. Schulz, *In situ Röntgenpulverbeugung an polykristallinem Silber und Kupfer in der Partialoxidation von Methanol.* PhD thesis, Technischen Universität Berlin, 2003. https://depositonce.tu-berlin.de/bitstream/11303/1076/1/Dokument_36.pdf, p. 39.

[15] D. Zagorac, H. Müller, S. Ruehl, J. Zagorac, and S. Rehme, "Recent developments in the Inorganic Crystal Structure Database: theoretical crystal structure data and related features," *J. Appl. Cryst.*, vol. 52, p. 918, 2019.

[16] H. T. Stokes and D. M. Hatch, "Program for identifying the space group symmetry of a crystal," *J. Appl. Cryst.*, vol. 38, p. 237, 2005.

[17] H. T. Stokes, D. M. Hatch, and B. J. Campbell, "FINDSYM – ISOTROPY Software Suite." web, 2021. iso.byu.edu.

[18] U. Martin, H. Boysen, and F. Frey, "Neutron powder investigation of tetragonal and cubic stabilized zirconia, TZP and CSZ, at temperatures up to 1400K," *Acta Cryst. B*, vol. 49, p. 403, 1993.

[19] G. Trolliard, D. Mercurio, and J. M. Perez-Mato, "Martensitic phase transition in pure zirocnia: a crystal chemistry viewpoint," *Z. Krist.*, vol. 226, p. 264, 2011.

[20] G. R. Hugo, "A crystallographic analysis of the tetragonal to monoclinic transformation in ZrO_2-12 mol % CeO_2," 1994.

[21] R. A. Evarestov and Y. E. Kitaev, "New insight on cubic–tetragonal–monoclinic phase transitions in ZrO_2: *Ab initio* study and symmetry analysis," *J. Appl. Cryst.*, vol. 49, p. 1572, 2016.

[22] T. Shimizu, K. Katayama, T. Kiguchi, A. Akama, T. J. Konno, O. Sakata, and H. Funakubo, "The demonstration of significant ferroelectricity in epitaxial Y-doped HfO_2 film," *Sci. Rep.*, vol. 6, p. 32931, 2016.

[23] C. Richter, M. Zschornak, D. Novikov, E. Mehner, M. Nentwich, J. Hanzig, S. Gorfman, and D. C. Meyer, "Picometer polar atomic displacements in strontium titanate determined by resonant X-ray diffraction," *Nature Commun.*, vol. 9, p. 178, 2018.

[24] C. Richter, “pyasf – symbolic computing of anisotropic resonant scattering factor.” web, 2021. https://github.com/carichte/pyasf.